Atmos. Chem. Phys. Discuss., 9, 9647–9691, 2009
www.atmos-chem-phys-discuss.net/9/9647/2009/

Atmospheric Chemistry and Physics Discussions

This discussion paper is/has been under review for the journal *Atmospheric Chemistry and Physics (ACP)*. Please refer to the corresponding final paper in *ACP* if available.

Application of φ-IASI to IASI: retrieval products evaluation and radiative transfer consistency

G. Masiello[1], C. Serio[1], A. Carissimo[1], G. Grieco[1], and M. Matricardi[2]

[1]Dipartimento di Ingegneria e Fisica dell'Ambiente, University of Basilicata, 85100 Potenza, Italy
[2]European Centre for Medium-Range Weather Forecasts (ECMWF), Shinfield Park, Reading, Berkshire, RG2 9AX, UK

Received: 22 February 2009 – Accepted: 2 April 2009 – Published: 16 April 2009

Correspondence to: G. Masiello (guido.masiello@unibas.it)

Published by Copernicus Publications on behalf of the European Geosciences Union.

Abstract

Retrieval products for temperature, water vapour and ozone have been obtained from spectral radiances measured by the Infrared Atmospheric Sounding Interferometer flying onboard the first European Meteorological Operational satellite. These products have been used to check the consistency of the forward model and its accuracy and the expected retrieval performance. The study has been carried out using a research-oriented forward-inverse methodology, called φ-IASI, that the authors have specifically developed for the new sounding interferometer. The performance of the forward-inversion strategy has been assessed by comparing the retrieved profiles to profiles of temperature, water vapour and ozone obtained by co-locating in space and time profiles from radiosonde observations and from the European Centre for Medium-Range Weather Forecasts analysis. Spectral residuals have also been computed and analyzed to assess the quality of the forward model. Two versions of the high-resolution transmission molecular absorption database have been used. Their performance has been assessed by inter-comparing the results.

1 Introduction

The study presents and describes the application of the φ-IASI package (Grieco et al., 2007) to the retrieval of temperature, moisture and ozone from IASI (Infrared Atmospheric Sounding Interferometer) data obtained during the commissioning phase of the instrument. The IASI data considered in this study were measured over the tropical basin. We have considered two datasets.

The first one is based on the Joint Airborne IASI validation experiment (JAIVEx) (Taylor et al., 2007), which was carried out in the United States during April and May 2007. Although limited in size, only 25 clear-sky very accurately calibrated IASI spectra were used, this is the most comprehensive data set we have, with time and space collocated radiosonde observations. It has been used for radiance closure and, hence,

to verify the quality and consistency of radiative transfer and spectroscopy.

The second dataset consists of 647 IASI spectra, which were measured during the IASI commissioning phase on 22 July 2007 over the tropical belts. For this second dataset of IASI observations, in-situ (truth) data have been derived from the ECMWF analysis for the same date and location as those of the IASI soundings. This second data set has been mostly used for an independent check of IASI retrieval accuracy.

To simplify the comparison of retrieval products with *truth* data, only clear-sky, sea-surface IASI soundings have been analyzed in this work.

To assess the retrieval performance of the physical inversion scheme we have evaluated differences between retrieved and in-situ profiles of temperature, water vapour and ozone. In addition, spectral residuals for each inversion have been computed and compared to the IASI radiometric noise. To this end we have used two versions of HITRAN (high-resolution transmission molecular absorption database), HITRAN 2000 (Rothman et al., 2003) and the most recent HITRAN 2004 (Rothman et al., 2005) with updates up to January 2007 (Gordon et al., 2007).

During the course of the study we have made extensive use of the forward module (that we call σ-IASI) (Amato et al., 2002), which consists of a monochromatic radiative transfer model which has been designed for the fast computation of spectral radiance and its derivatives (Jacobian) with respect to a given set of geophysical parameters.

Of equal relevance to the present study is the inverse module of the φ-IASI package, which we call δ-IASI (Carissimo et al., 2005). This is a physical-based inversion algorithm for the retrieval of geophysical parameters (skin temperature, temperature, water vapour and ozone profiles, columnar amount of trace species such as methane, carbon monoxide and nitrous oxide) from high-resolution infrared radiance. The inverse package incorporates its own forward module (σ-IASI), therefore it involves an end-to-end procedure, which from the input observed spectral radiance leads to the retrieved geophysical parameters, without any further intervention of the user. For the present study, an optimized serial version (Carissimo et al., 2009) of the forward radiative transfer model, σ-IASI, has been developed which is more computationally efficient

(about 100 times faster) that the original version of the software. A parallelized version of the software has also been developed that can achieve a very good scalability with the number of available processors.

Rather than for operational purposes, the package φ-IASI is intended for providing a kit of models to address research issues on inversion methodology (including Tikhonov and/or Rodgers regularization, Levenberg-Marquardt least-square minimization) and radiative transfer (including generation of analytical derivative matrices, impact of new spectroscopy). It has been extensively validated using NAST-I spectra (Cousins and Gazarick, 1999, e.g.). NAST-I is the NPOESS Airborne Sounder Testbed Fourier Transform spectrometer flying onboard the NASA ER-2 and Proteus aircrafts. An extensive retrieval exercise with σ-IASI has been carried out using datasets from the CAMEX/3 experiment (Convection and Moisture Experiment 3), (Carissimo et al., 2005, 2006, e.g.). More recently, φ-IASI has been used during the EAQUATE campaign (European AQUA Thermodynamic Experiment), to analyze NAST-I spectra (Proteus Flight) measured over the Mediterranean Sea (Taylor et al., 2008; Grieco et al., 2007). The forward module σ-IASI has also been validated using radiances from the Atmospheric Infrared Sounder (AIRS) instrument flying onboard the Aqua satellite (Saunders et al., 2007).

The paper is organized as follows. In Sect. 2 we describe the basic aspects of the forward-inverse methodology, φ-IASI. In Sect. 3 we describe the data used in the study and discuss the results. Conclusions are drawn in Sect. 4

2 The φ-IASI package and its expected performance for IASI

The φ-IASI package has been extensively documented in the open literature (Amato et al., 2002; Carissimo et al., 2005; Grieco et al., 2007) and it includes

- a stand alone cloud detection scheme (Masiello et al., 2003);
- an Empirical Orthogonal Function (EOF) regression scheme for the computation of the first guess state of the atmosphere, which is used for the initialization of the

non-linear physical inversion, (Grieco et al., 2005, 2007; Serio et al., 2009);

- a suitable forward module, σ-IASI (Amato et al., 2002; Masiello and Serio, 2003; Grieco et al., 2007);
- a suitable inverse scheme, δ-IASI (Carissimo et al., 2005; Grieco et al., 2007).

Here we discuss the basic aspects of the forward and inverse modeling, which are relevant to the present analysis.

2.1 The forward model, σ-IASI

It consists of a monochromatic radiative transfer model which has been designed for the fast computation of spectral radiance and its derivatives (Jacobian) with respect to a given set of geophysical parameters.

The forward module computes monochromatic radiances from look-up tables of monochromatic layer optical depth generated using the line-by-line model LBLRTM (Clough et al., 2005).

Cross sections of heavy molecules such as chlorofluorocarbons are parameterized in terms of different look-up tables, since absorption can be quickly computed separately. The code σ-IASI can include the presence of CFC's species, namely CCl3F (CFC-11) and CCl2F2 (CFC-12). Water vapour continuum absorption is computed separately using the scheme by Clough et al. (1989). In addition, σ-IASI takes into account the self-broadening effect of water vapour (Masiello and Serio, 2003) which is particularly relevant to the present study. The atmospheric layering implemented in σ-IASI consists of a pressure layer grid of N_L =60 grid points. The definition of the model pressure levels is in Table 1.

Recent important improvements of σ-IASI include (Carissimo et al., 2009) a new analytical scheme for the computation of the radiance derivative with respect to H_2O mixing ratio, q which takes into account the non-linearity of the spectral optical depth

ACPD
9, 9647–9691, 2009

with respect to q introduced by a) continuum absorption, and b) self-broadening absorption effect. Other new features include also the parallelization of the code that now can run almost in real time.

For the present version of σ-IASI, the required look-up tables have been generated with two different versions of LBLRTM,

- LBLRTM version 8.1, in which line parameters are taken from HITRAN 2000 including the 2001 modifications (Rothman et al., 2003). The continua come from MT_CKD version 1.0 (Tobin et al., 1999). The resulting σ-IASI version will be referred to in the following as release L8.1, or σ-IASI_L8.1.

- LBLRTM version 11.3, released on November 2007. In this newest version the line parameters are obtained from the compilation aer_v_2.1 developed by AER Inc. of Massachusetts, USA (AER, 2007). This line compilation is derived from HITRAN 2004 (Rothman et al., 2005) and includes updates up to 1 January 2007 (e.g. for the water vapour it includes the diet of the air-broadened half-widths, Gordon et al., 2007). For the IASI spectral range the only differences between aer_v_2.1 and HITRAN2004 database are for the Carbon dioxide lines. In order to be consistent with the line coupling parameter derived by Niro et al. (2005), AER database uses the 2000 version of Carbon Dioxide line parameters. Furthermore, the continua adopted in LBLRTM v. 11.3 are the latest public release of the MT_CKD model. This version 2.1, for the water vapour, take into account the new values of the half-widths, while, as said above, the continuum for carbon dioxide has been calculated based on the new line coupling model developed by Niro et al. (2005). The resulting σ-IASI version will be refereed to in the following as release L11.3, or simply σ-IASI_L11.3.

To generate IASI synthetic spectra, the σ-IASI infinite resolution spectrum has to be convolved with the IASI Instrumental Spectral Response Function. This is better defined in the interferogram domain, where it can be expressed as a truncated Gaussian,

$G(x)$ given by

$$\begin{cases} G(x) = \exp\left(-\frac{x^2}{2v^2}\right) \text{ if } -x_{co} \leq x \leq x_{co} \\ G(x) = 0 \text{ otherwise} \end{cases} \quad (1)$$

with the optical path difference, x in units of cm and

$x_{co} = 1.9679466\,\text{cm}$

$$v^2 = \left(\pi^2 \sigma_o^2\right)^{-1} 2\log(2). \quad (2)$$

The IASI ISRF, $F_G(\sigma)$ in the spectral domain is obtained by Fourier transforming the function, $G(x)$.

$$F_G(\sigma) = \int_{-\infty}^{+\infty} G(x) \exp(-2\pi i x \sigma) dx. \quad (3)$$

The parameter σ_o, appearing in (2), determines the Full-Width Half-Maximum (FWHM) of $F_G(\sigma)$. The choice for IASI is $\sigma_o = 0.5\,\text{cm}^{-1}$.

2.2 The inverse model δ-IASI

Of particular relevance to the present study is the inverse module of the φ-IASI package, which we call δ-IASI (Carissimo et al., 2005; Grieco et al., 2007). This is a physical-based inversion algorithm for the retrieval of geophysical parameters (temperature, water vapor and ozone) from highly resolved infrared radiances. The inversion package incorporates its own forward module (i.e. σ-IASI), therefore it can be considered as an end-to-end procedure, which, given the input observed spectral radiance, returns the geophysical parameters without any further intervention of the user.

The inverse module, δ-IASI implements a non-linear inversion procedure and, therefore, it has to be properly initialized. For the present study, the initialization is provided

ACPD
9, 9647–9691, 2009

by the Empirical Orthogonal Function (EOF) statistical retrieval approach described in (Grieco et al., 2005; Serio et al., 2009).

The basic implementation of the inverse scheme follows Rodgers's statistical regularization method (Rodgers, 1976). However, an additional regularization parameter, γ is introduced in the inverse scheme which gives to the algorithm the capability of improving the retrieval accuracy and constrains the step size of Newton updates in such a way as to iterate towards the likely region of the inverse solution (Carissimo et al., 2005; Grieco et al., 2007). Within δ-IASI, this additional regularization parameter can be chosen or changed in such a way to allow various inversion modes. By selecting γ=1, we can implement the usual Rodgers's scheme. In this work γ has been optimized by resorting to the well-known L-curve criterions (Hansen, 1992).

For the work here shown, the following spectral ranges have been considered for the inversion of IASI data,

- 645 to 810 cm^{-1};
- 1010 to 1080 cm^{-1};
- 1100 to 1200 cm^{-1};
- 1450 to 1600 cm^{-1};
- 2000 to 2230 cm^{-1}.

At the IASI sampling rate of 0.25 cm^{-1}, this corresponds to a number of IASI spectral radiances, n=2865. The spectral location of these channels is shown in Fig. 1, which also allows us to exemplify the spectral quality of IASI data.

To apply δ-IASI to the observations, we need the IASI observational covariance matrix, **C**. For the present work, this has been assumed to be diagonal and computed according to

$$\mathbf{C}=\mathbf{O}+\mathbf{F} \tag{4}$$

ACPD
9, 9647–9691, 2009

with **O** the observational covariance matrix made up with the apodized level 1C IASI radiometric noise. The reader interested to understand the effect of apodization over noise and retrieval is referred to Amato et al. (1998).

The matrix **F** models the forward model noise, and for the work here presented **F** is chosen to be proportional to **O**,

$$\mathbf{F}=f^2\mathbf{O} \tag{5}$$

where f is a tuning parameter, which can be properly scaled in order to yield a final iterate, which produces a χ^2 value below a given thresholds, χ^2_{th}. The χ^2 function is here defined as usual

$$\chi^2=\delta\mathbf{R}^t\mathbf{C}^{-1}\delta\mathbf{R} \tag{6}$$

where $\delta\mathbf{R}$ is the spectral residual defined as observed minus calculated radiances.

A normal δ-IASI run is assumed to have attained to a converged solution, when the calculated χ^2 is below χ^2_{th}, which for the analysis at hand is set equal to a χ^2 variable with n degrees of freedom at a tolerance limit of 95%. If we work with normalized quantities χ^2/n, then the threshold is simply, $\chi^2_{\text{th}}/n\approx 1$. Normally, the degrees of freedom, n are equal to the number of spectral radiance data points or, equivalently, the size of the radiance vector, **R** minus the number of parameters estimated from the radiance vector itself for the generation of the first guess. The number of these parameters is equal to the number of EOF scores that in our scheme is normally 12, 14 and 25 for temperature, water vapour and ozone, respectively. Because of the orthogonality property of principal components, we estimate from the radiance vector a total of parameters given by $\max(12, 14, 25)=25$. This figure may be compared with the number of spectral radiance data points, $n=2865$.

With the above fitting procedure we can assess the degree of consistency among observations and computations and a measure of this consistency is just the index f^2. The case $f^2=0$ corresponds to a perfect forward model. The larger f^2 is and the higher the inconsistency is. This simple procedure allows us to measure the inconsistency in

terms of an additive source of pseudo noise, which may be compared directly to the size and magnitude of the IASI radiometric noise.

As said before, this pseudo noise mostly arises from forward modeling error, which, in turn, may have different sources: error in representing continuous parameters of altitude (such as temperature, water vapour and ozone) with discrete functions defined on a pressure/altitude mesh of atmospheric layers, residual cloud contamination in the radiances, uncertainty in the surface emissivity and trace gases that are not in the set of retrieved parameters, parameterizations of monochromatic transmittances in look-up tables, and last but not least spectroscopy errors in absorption line positions and strengths and related continua.

Because we know that there is a forward model noise, it is not prudent to yield inversions with $f=0$, since we could experience biases in the retrieval because of data overfitting. The choice of f is a matter of trial and error and depends on the quality of data and spectroscopy. As an example for the JAIVEx data we were able to run with $f^2=0.96$, a rather small value, which is likely the result of the careful inspections for calibration of IASI spectra and highly confident clear sky IASI field of view obtained for this experiment. For the case of the second set of IASI data, which we had to retrieve directly from EUMETcast and qualify for clear-sky with a IASI stand alone cloud detection algorithm, we were able to run with a value of $f^2=3\div5$.

2.2.1 δ-IASI expected performance for IASI

The expected retrieval performance for IASI of the inverse scheme has been assessed in simulation using the Chevalier data base (Chevalier, 2001) for temperature, water vapour and ozone, *(T,q,o)* profiles. For the analysis here shown we have considered only clear-sky sea-surface and tropical profiles. This subset is made up of 377 individual profiles for *(T,q,o)* and has been also used to train the EOF statistical initialization scheme.

Normally, δ-IASI retrieves the skin temperature and *(T,q,o)* profiles. The other atmospheric parameters are set to their climatological values. For gas species concentra-

tions we use the compilation by Anderson et al. (1986); the surface emissivity is that derived by Masuda's model (Masuda et al., 1988) for sea surface and a mean wind speed of 5 m/s.

In performing the simulation exercise we have assumed a perfect knowledge of spectroscopy and forward model, so that the performance shown in Figs. 2 to 4 has to be intended as the best performance we could achieve with our methodology.

Figure 2 shows the expected retrieval accuracy for temperature. The figure shows the root mean square error, r as obtained after the EOF regression and the final physical inversion. For comparison the standard deviation of the ensemble of the 377 test profiles is shown, as well. The root mean square error, $r(p)$ at any given pressure-layer, p is computed as usual,

$$r(p)=\left[\frac{1}{m}\sum_{i}^{m}\left(X_r(p;i)-X_t(p,i)\right)^2\right]^{1/2} \tag{7}$$

where $X(p,i)$ indicates a generic retrieved parameter at pressure, p and i labels the number of test cases, $i=1,\ldots,m$, with $m=377$. In a similar way we also compute the bias, $b(p)$

$$b(p)=\frac{1}{m}\sum_{i}^{m}\left(X_r(p;i)-X_t(p,i)\right). \tag{8}$$

It is interesting to see, from Fig. 2, that the EOF regression improves the performance over the simple estimate given by the mean value of the training data set and that the physical inversion improves at any altitude level the accuracy of the retrieval. Based on the physical inverse scheme estimate, the expected temperature retrieval accuracy for IASI is quite close to the goal accuracy od 1 K in the troposphere. Also interesting to note is that the bias (shown in Fig. 5a) is confined to one tenth of K along the whole troposphere and lower stratosphere.

Figure 3 shows the expected water vapour retrieval performance. Again based on the final physical inversion, the root mean square error in the lower troposphere ranges in

ACPD
9, 9647–9691, 2009

between 1 to 1.5, this corresponds to a percentage error of 10% to 20%, which is larger than the goal accuracy of 10%. It is important to stress here that our retrieval scheme uses mostly information from the data themselves. We do constrain the solution with a sort of climatology derived from the Chevalier data set, but this imposes a rather loose constraint to the final solution. In addition, we remark that what is shown in Fig. 3 is the best achievable performance with our method. In other words, unless the data are bounded with much more informative constraints, such as done in the normal practice of a data assimilation system, which uses, e.g., forecast fields available from Numerical Weather Prediction centers, IASI will not perform better than 10–20%, as far as the retrieval accuracy of water vapour is concerned. Moreover, for H_2O the bias oscillates between ±0.3 g/kg in the lower part of the atmosphere (see Fig. 5b), a value which is almost negligible once compared to the typical concentrations of this gas in tropical settings. Furthermore, the integral of this bias along the atmospheric column tends nearly to zero, which means that the columnar amount is largely unbiased.

For ozone, the expected performance is shown in Fig. 4. The root mean square error is confined below 10% in the region where we normally observe the bulk concentration of this atmospheric gas. It is interesting to note that the magnitude of bias (shown in Fig. 5c) is in any case fairly low and tend to oscillate around the zero line, which means that the retrieved atmospheric columnar amount of ozone is fairly unbiased. However, for the case of ozone it is fair to observe that the very good performance could be an artifact of the limitations of the test data set (the Chevalier data base), which for the case of ozone is made up of very smooth vertical profiles.

The analysis of the spatial vertical resolution of the retrieved profiles that are produced by δ-IASI has been discussed at a length in various papers. A comprehensive discussion can be found in Grieco et al. (2007). The analysis shows that retrieved profiles tend to be highly correlated along the vertical.

In addition to the well known, and sometimes abused, methodology of averaging kernels (which dates back to Backus and Gilbert, 1968) the interdependency along the vertical of the retrieved parameters can be assessed with the help of the i_D index in-

troduced by Serio et al. (2008, 2009). This index works on the a-posteriori covariance matrix of retrieval and may assume values from 1 to N_L, with N_L the number of atmospheric layers used to render the vertical profile of the given parameter. In other words, N_L is the size of the generic inverted vector, $\boldsymbol{X}_r$ (for our analysis N_L=60).

The value, i_D=1 simply means that for the retrieval at hand it is as if the full atmosphere had been divided just in one layer, that is only the columnar amount of the parameter has been resolved. On the opposite edge of the i_D scale, we have i_D=N_L, and the retrieval has been fully resolved on the grid mesh used to divide the atmosphere. Nearby layers can then, e.g., be used to form average quantities and, therefore, reduce the estimation error.

For the simulation exercise at hand, if we denote with δX the difference (retrieval-test) for the generic parameter X, then the a-posteriori covariance matrix can be estimated by considering the expectation value of $(\delta\mathbf{X})(\delta\mathbf{X})^t$. Then, the i_D index can be easily computed from this matrix (Serio et al., 2008, 2009). We have found

- i_D=6.3 for temperature;
- i_D=4.3 for water vapour;
- i_D=2.9 for ozone.

These values say that much of the information in the IASI data is reserved to temperature, less for water vapour and even less for ozone. However, for ozone it is important to stress that IASI is capable of three pieces of information, a result which is also confirmed in the recent work by Emerenko et al. (2008). The modest value for H_2O says that only very coarse features of the water vapour profile are within the IASI capability.

3 Application to IASI data and results

3.1 IASI and truth data

As said before, we are dealing in this study with two sets of IASI data:

1. the first set has been derived from the 2007 JAIVEx campaign (see Taylor et al., 2007 for more details) over the Gulf of Mexico. We have a series of 6 spectra for the day 29 April 2007, 16 spectra for the day 30 April 2007, and finally 3 spectra for the day 4 May 2007. The total of 25 soundings are well collocated with radiosonde observations, as shown in Fig. 6. The spectra where recorded for clear sky fields of view, selected based on high resolution satellite imagery from AVHRR (Advanced Very High Resolution Radiometer) on MetOp (Meteorological Operational Satellite) and in-flight observations. Furthermore, the data for the day 29 April 2007 correspond to a nadir IASI field view, whereas those for the other two days to a field of view of 22.50 degrees.

2. A second data set has been acquired during the IASI commissioning phase on 22 July 2007. The geo-location of these soundings can be seen in Fig. (7). In total, a number of 647 IASI spectra has been selected. The spectra have been observed on sea surface and refer to nadir looking mode and clear sky conditions. Clear sky was checked using the cloud detection scheme described in (Masiello et al., 2003; Grieco et al., 2007). This second set of data will be referred to as simply the *tropical set*.

For the tropical set, in order to develop a consistent set of truth data against which IASI retrieval could be compared, ECMWF atmospheric analysis fields for temperature, water vapor and ozone were considered. These fields where time and spatially co-located to the 647 IASI soundings. We used atmospheric analysis fields of 00:00, 06:00, 12:00, 18:00 and 24:00 UTC on 22 July 2007.

At that time, the ECMWF model was characterized by a vertical discretization of the atmosphere into 60 pressure levels and a horizontal truncation of T511. This truncation corresponds to a grid spacing of about 40 km or, equivalently, to a horizontal grid box of $0.351^{\circ} \times 0.351^{\circ}$. The model has a hybrid vertical coordinate, with terrain-following co-ordinates in the lower troposphere and pressure coordinates in the stratosphere above about 70 hPa. Of the 60 levels in the vertical, 25 are above 100 hPa and the model top is

ACPD
9, 9647–9691, 2009

at 0.1 hPa, corresponding to about 65 km. The vertical resolution of the analysis fields gradually decreases from 20 m at the surface to about 250 m at 1 km altitude, and about 1 km to 3 km in the stratosphere. The analysis fields were extracted from the ECMWF archive at the full T511 resolution, interpolated to a grid of points with a separation of 0.3°× 0.3°and then co-located to the IASI soundings. The statistics of the difference between global radiosonde observations and ECMWF analysis in the troposphere show values of the standard deviation typically between 0.5 K and 1 K for temperature and between 0.5 and 1.5 g/kg for water vapour. In addition to fields of temperature, water vapour and ozone, ECMWF fields of sea-surface temperature (SST) were also used in the study. It should be noted that these fields are based on analyses received daily from the National Centers for Environmental Prediction (NCEP), Washington DC, on a 0.5°× 0.5°grid. These analyses are based on ship, buoy and satellite observations. In shallow waters, where rapid changes due to the upwelling radiation can occur close to land, the observed SST can sometimes differ as much as 5 K from the NCEP analysis.

3.2 Results: radiance closure experiment and forward modelling consistency as derived from JAIVEx data

As anticipated, the analysis performed in this study have been carried out with two different releases of δ-IASI, which use different version of the forward model: namely σ-IASI_L8.1 and σ-IASI_L11.3. The reader is referred to Sect. 2.1 for the details about the difference between these two implementations.

The two δ-IASI packages have been used to yield inversions for temperature, water vapour and ozone from the 25 JAIVEx spectra. As a by product, the process produces also the corresponding 25 best-fit synthetic spectra, computed on the basis of the final retrieved state vector. Observations and best fitted spectra have been used to compute the spectral residual.

The spectral residual is defined according to

$$\delta\mathbf{R}=\mathbf{R}_{\text{iasi}}-\mathbf{R}_{\text{fit}} \quad (9)$$

with **R** the spectral radiance and the subscripts iasi and fit denote the observation and the fitted spectrum at the end of the inversion procedure.

The spectral residual, averaged over the full set of 25 JAIVEx IASI soundings is shown in Fig. 8 for the two runs, that is σ-IASI L8.1 and L11.3, respectively. To possibly improve the reading of the spectral residual, we also provide in Fig. 9 the spectral residuals in units of brightness temperature (K), for the range 645 to 2250 cm^{-1}, which is the range we use in our inversion methodology.

3.2.1 σ-IASI version L8.1

It is immediately seen from Fig. 8 (or equivalently Fig. 9) that the mean spectral residual (shown in Fig. 8a for the case L8.1) does not tend to zero as it should be for an ideal case in which we had a perfect forward model. For comparison, Fig. 8a also shows the IASI radiometric noise. Because we have averaged 25 spectra, in case of a perfect random noise, the mean spectral residual should be a factor of $\sqrt{(25)}$=5 lower that the IASI radiometric noise. This is not the case, and we remark that in order to achieve convergence of the inversion procedure, within the χ^2 metric, we had to put f^2=0.96 (see discussion in Sect. 2.2.1). This means that the forward model noise is about one half of the IASI radiometric noise.

However, this additional source of noise is not random. In fact, from Fig. 8a we see that it is strongly patterned and the shape of the patterns follow the shape of the various absorption bands.

One pattern is most evident from Fig. 8a, which exceeds the IASI noise. It coincides with the methane absorption band, centered at 1350 cm^{-1}. The large misfit is due to the fact that it is not included among the retrieved parameters. A second, less evident discrepancy is seen in the CO weak band in the short wave side of the IASI spectrum at 2140 cm^{-1}. Again, carbon monoxide was not included within the retrieved parameters. For both methane and carbon monoxide we used climatology.

For the CO_2 ν_2-band at 667 cm^{-1}, we have that the spectral residual is comparable with the IASI noise. Nevertheless it is patterned and not symmetric around zero. The

patterns also follow the signature of absorption lines.

For the ozone band at 1040 cm^{-1} we also see a relatively large inconsistency, with marked signatures which are likely due to a lack of correct spectroscopy.

For water vapour, we still see an imperfect rendering of absorption features from the forward model. Also evident, across all the absorption band at 6.7 μm, is a slight but consistent hot bias, which is likely a problem of H_2O continuum.

Nevertheless, the retrieval performance is fairly good for both temperature and water vapour, as it is possible to see from Fig. 10, which shows the results for the day 30 April 2007, for which we have the largest set of spectra. The performance is in line with what expected from the simulation analysis we have shown in Sect. 2.2.1. The root mean square error shown in Fig. 10 has been calculated by contrasting retrievals against the radiosonde observations.

3.2.2 σ-IASI version L11.3

The spectral residual, averaged over the 25 IASI soundings, for the case L11.3 is shown in Fig. 8b (see also Fig. 9b). By comparing to Fig. 8a (and Fig. 9a), we see a fair improvement for the ozone band at 1040 cm^{-1} and more modest one for the H_2O ν_2-absorption band at 1600 cm^{-1}. In addition we see an improvement in the range 700 to 800 cm^{-1} of the CO_2 ν_2-absorption band. This is the most consistent and striking improvement we see with the version L11.3 in comparison to the older L8.1. We think that this is a direct effect of the fact that for the version L8.1 we have only Q-branch line mixing treatment, whereas for the version L11.3 that uses the new model by Niro et al. (2005), the treatment extends up to include all P,Q and R lines.

However, apart the aforementioned improvement, we see a serious degradation for the range 645 to 700 cm^{-1}, which is better evidenced in Fig. 11, which shows a close up of this spectral range. From this last figure a much severe inconsistency is seen at the centre of the CO_2 Q-branch at 667 cm^{-1}.

The inconsistency of L11.3 is also very well reflected in the temperature retrieval

ACPD
9, 9647–9691, 2009

accuracy shown in Fig. 10a. It is seen from this figure that the retrieval exhibits a large misfit just below the tropopause, in the pressure range 100 to 200 mbar. This part of the altitude range is extremely sensitive to the spectral range 640 to 700 cm^{-1}, as it is also possible to understand from analyzing the Jacobian for temperature. An analysis that is not shown here just for the sake of brevity.

A series of checks we performed by changing and tuning spectroscopic parameters for the range 640 to 800 cm^{-1} led us to conclude that the L11.3 inconsistency shown in Fig. 11 is due to the stronger CO_2 continuum absorption for the range 640 to 700 cm^{-1} than that provided by L8.1.

As said in Sect. 2.1, since the CO_2 continuum depends on line coupling treatment, the version L11.3 has a different continuum compared to the version L8.1.

The two continua for L8.1 and L11.3 are exemplified in Fig. 12 for the CO_2 $v2$ band. It is should here stressed that the two releases at hand are based on the same HITRAN 2000 line compilation for CO_2. Therefore intensity and position of lines for L11.3 are the same as those for L8.1. Therefore, although the line mixing scheme is different, the two continua can be at least compared to understand the origin of the retrieval misfit caused by L11.3 in comparison with L8.1, which, we stress, yields a better performance for temperature. From Fig. 12 it is seen that L11.3 CO_2 continuum is much more absorbing at the band centre of the CO_2 ν_2 absorption spectral region.

This excess of continuum absorption is also evidenced by the behaviour of IASI and fitted spectra at the bandhead of the CO_2 ν_3 spectral region. The comparison provided in Fig. 15 tends to confirm an excess of continuum absorption of L11.3 in comparison to L8.1. In fact, this figure clearly shows that L11.3 is much more inconsistent with IASI than L8.1

At this point, trying to understand the right direction towards which to move in order to decrease the misfit in spectral residual and retrieval, we have attempted to adjust the L11.3 continuum trough the simple model

$$c_{new}(\sigma)=c_1(\sigma)+a\,[c_2(\sigma)-c_1(\sigma)]\,; \quad (10)$$

where $c_{new}(\sigma)$, $c_1(\sigma)$ and $c_2(\sigma)$ denote the new continuum, the continuum absorption

for the version L8.1 and L11.3, respectively.

By changing a in the range 0 to 1, we can move from L8.1 to L11.3 continuum. All our attempts to optimize a on the basis of IASI spectra, through minimization of both the spectral residual for the spectral range 645 to 700 cm^{-1} and temperature misfit for the pressure range 100 to 200 mbar (see again Fig. 10a) led us to $a \approx 0$.

Our δ-IASI inversion scheme does not use the CO_2 ν_3 band, so that we could not simultaneously compromise between ν_2 and ν_3. Thus, $a=0$ is the best compromise for the ν_2 band alone. However, our findings clearly identify a too much strong absorption at the ν_2 band center, which gives a very high residual for the Q-branch at 667 cm^{-1}.

At this point it is important to stress that the version L11.3 for the CO_2 continuum has been derived for a temperature of 296 K. Furthermore, this continuum does not include any dependence on the temperature itself (e.g. see Shephard et al., 2009), whereas heavily insists on line-mixing collisional effects. These effects yield a continuum which has a very strong super-Lorentzian behaviour at the core of the band (667 cm^{-1}) and a sub-Lorentzian behaviour in the band-wing (e.g. see again Fig. 12). However, at the typical temperature and pressure of the tropical stratosphere, line mixing is expected to have much little role than in the lower troposphere, therefore the appropriate continuum for the stratosphere altitude range should have a behaviour in between a pure Lorentzian and a collisional continuum. According to our results, it seems that this kind of continuum is provided by L8.1, which is based on an effective chi factor. This fact is likely to explain the better performance of L8.1 continuum with respect to that of L11.3 and suggests that the continuum for CO_2 should be defined and computed by properly accounting for altitude, temperature and pressure range.

Based on our results we implemented a third version of σ-IASI, which will be referred to in the following as σ-IASI_L11.3_s, in which the L11.3 continuum for CO_2 is substituted with the L8.1 ones.

This new version achieves the best spectral consistency, not only for the range 640 to 700 cm^{-1}, but also for the full coverage we used for inversions (see, e.g. Figs. 13 and 14), and improves the temperature retrieval as it is possible to see from Fig. 10.

ACPD
9, 9647–9691, 2009

3.3 Inversion results for the tropical data set

The tropical data set of 647 IASI spectra deserves as an independent set of data, which can be used to check the benefit introduced by the three releases at hand. The IASI spectra were inverted for skin temperature, temperature, water vapour and ozone profiles. Retrievals were obtained for the three versions of σ-IASI we are dealing with in this paper: L8.1, L11.3 and L11.3_s.

Figures from 16 to 18 summarizes the performance of the scheme for temperature, water vapour and ozone, respectively. The performance has been quantitatively evaluated by considering, for any pressure level, p, the bias, $b(p)$ and the root mean square difference, $r(p)$, defined as in Eqs. (7) and (8), where now the role of the test profiles is played by the ECMWF profiles, and the number of test cases is m=647.

For temperature we have that the bias is confined within ±1 K in the lower troposphere, where the root mean square difference ranges in between 1–2 K. Considering that ECMWF temperature profile is credited of an accuracy within 0.5–1 K, the results we have found are quite close to the expected accuracy of 1 K for the troposphere.

Figure 16 also allows us to compare the performance achieved with the various σ-IASI version. In this respect, it is seen that L11.3_s achieves the best root mean square error and yields the smaller bias in the lower troposphere. L11.3 gets the worse performance in the upper part of the troposphere, which once again evidences a non perfect match between line and continuum absorptions in the latest LBLRTM version. L11.3 yields also largely biased retrievals in the upper part of the troposphere, in between 100 to 400 mbar, which again confirms a non proper scaling of the CO_2 continuum for this version. In fact, the bias is partly removed and the performance increased to the level of that allowed by L8.1 and better, when we consider the version adjusted for the CO_2 continuum absorption, that is L11.3_s. This suggests that our scaling of the CO_2 continuum goes in the right direction and should be used to improve LBLRTM 11.3 until a new and more appropriate continuum is developed.

For water vapour (shown in Fig. 17) the shape of bias and root mean square differ-

ACPD
9, 9647–9691, 2009

ence are quite similar to those obtained in simulation and discussed in the previous Sect. 2.2.1, although their magnitude increase in comparison to those values. Also for this case considering the accuracy of the ECMWF analysis, the performance for water vapour is fairly close to what expected based on the simulation exercise. As far as the difference between the three versions of the forward module, we have that the most updated, L11.3_s shows a modest, improvement over the older L8.1. This in part is the clue for a better temperature retrieval in the lower part of the atmosphere and a better water vapour spectroscopy.

For the case of ozone (see Fig. 18), we have that the difference with the ECMWF analysis is mostly made up of bias. Finally, for this case L11.3_s shows degradation with respect the older L8.1. However, inspection of residuals show that L11.3_s achieves a better consistency with IASI spectra.

Finally, it is important to stress that the we could obtain converged retrieved solutions, in the χ^2 sense (see Sect. 2.2.1) only by a proper tuning of the inconsistency factor, f^2. For both L8.1 and L11.3_s we could run with f^2=3. However, this factor had to be increased to 5 for the case of L11.3, which confirms the relative strong inconsistency of the present formulation for the CO_2 continuum in LBLRTM v. 11.3.

4 Conclusions

We have performed a series of retrieval exercises using IASI tropical soundings, two different compilations for absorption line and continuum parameters, three different implementations of a fast forward model, built upon a state-of-art radiative transfer model.

State of art radiative transfer is consistent with IASI provided we introduce a forward modeling pseudo-noise whose magnitude is 0.5 to 2.5 times the current IASI radiometric noise. However, this noise shows a non-random component whose analysis allows us to have very clear diagnosis about where and how spectroscopy fails and, therefore, has to be improved in order to yield a better consistency among observations and

ACPD
9, 9647–9691, 2009

calculations.

Our findings say that mostly continuum absorption parameters for the fundamental CO_2 ν_2 and ν_3 bands have to be improved. Ozone still exhibits a relative large misfit with observations. Finally, water vapour absorptions parameters seem to be of enough quality to produce a negligible bias, at least in the spectral residual. However, also in this case line and continuum absorptions need to be improved.

A said before, a relative large discrepancy, confined in the CO_2 ν_2 and ν_3 bands, has been found between IASI and the synthetic spectra obtained through the latest LBLRTM version 11.3, seemingly because of an inappropriate CO_2 continuum absorption for the upper part of the atmosphere. This problem has been empirically alleviated for now by simply replacing the present continuum model for CO_2 in the LBLRTM version L11.3, with the CO_2 continuum from the older L8.1 model. However, better results are expected by developing a CO_2 model with the appropriate dependence on temperature and pressure. On this respect, comparable results and conclusion have been reported also by LBLRTM people (see e.g. Shephard et al., 2009).

As far as the accuracy of retrieval is concerned, it has been shown that state-of-art radiative transfer allows us to invert IASI data for temperature with an accuracy quite close to the goal performance of 1 K in the troposphere. For water vapour we are in a range of accuracy for the lower troposphere around 10 to 20%. However, even improving the accuracy of radiative transfer, the goal accuracy of 10% in the lower troposphere appears very difficult to achieve.

Once compared to simulations, real retrievals show a comparable root mean square error. However, compared to simulations the bias goes up and becomes the dominant factor in the root mean square error. This bias is the result of the aforementioned forward modeling pseudo noise, which demands for new basic research in order to be zeroed. In this context, the very good quality of IASI data could play a significant role, both for the assessment of this bias and to lead to suitable semi-empirical schemes to remove such a systematic component from forward models.

Finally, as far as the retrieval accuracy is concerned, our results also compare to

those shown by other authors (see e.g. Zhou et al., 2009), although our findings hint at a better performance for temperature and water vapour. However, it should be stressed that our methodology is not intended for operational purposes, as it is the case for other schemes. The package φ-IASI is mostly intended to address remote sensing research issues, and to get insight into understanding the capability of modern infrared satellite sensors and the impact of possibly new and improved spectroscopy.

Acknowledgements. IASI has been developed and built under the responsibility of the Centre National d'Etudes Spatiales (CNES, France). It is flown onboard the Metop satellites as part of the EUMETSAT Polar System. The IASI L1 data are received through the EUMETCast near real time data distribution service. We thank S. Newman (Met Office) for providing the JAIVEx data. The JAIVEx project has been partially funded under EUMETSAT contract Eum/CO/06/1596/PS. The FAAM BAe 146 is jointly funded by the Met Office and the Natural Environment Research Council. The US JAIVEx team was sponsored by the National Polar-orbiting Operational Environmental Satellite System (NPOESS) Integrated Program Office (IPO) and NASA.

References

AER: http://www.rtweb.aer.com/line_param_frame.html, access: 15 April 2009. 9652

Amato, U., De Canditiis, D., and Serio, C.: Effect of Apodization on the Retrieval of Geophysical Parameters from Fourier-Transform Spectrometers, Appl. Optics, 37, 6537–6543, 1998. 9655

Anderson, G. P., Clough, S. A., Kneizys, F. X., Chetwind, J. H., and Shettle, E. P.: AFGL Atmospheric concentration profiles (0–120 km), AFGL-TR-86-0110, AFGL (OPI), Hanscom AFB, MA 01736, USA, 1986. 9657

Amato, U., Masiello, G., Serio, C., and Viggiano, M.: The σ-IASI code for the calculation of infrared atmospheric radiance and its derivatives, Environ. Modell. Softw., 17/7, 651–667, 2002. 9649, 9650, 9651

Backus, G. and Gilbert, F.: The resolving power of gross Earth data, Geophys. J. Roy. Astr. S., 16, 169–205, doi:10.1111/j.1365-246X.1968.tb00216.x, 1968. 9658

Carissimo, A., De Feis, I., and Serio, C.: The physical retrieval methodology for IASI: the δ-IASI code, Environ. Modell. Softw., 20, 1111–1126, 2005. 9649, 9650, 9651, 9653, 9654

Carissimo A., Grieco G., Serio C., Cuomo V., Masiello, G. and Smith, W. L.: Application of sigma-IASI to NAST-I, Current problems in atmospheric radiation (IRS 2004): Proceedings of the International Radiation Symposium (IRC/IAMAS), Busan, Korea, 23–28 August 2004, A. Deepak Publishing, Hampton, VA, USA, 247–250, 2006. 9650

Carissimo, A., Grieco, G., Masiello, G., Matricardi, M., and Serio, C.: Application of the σ-IASI radiative transfer model to IASI, Current problems in atmospheric radiation (IRS 2008): Proceedings of the International Radiation Symposium (IRC/IAMAS), Foz do Iguau, Brazil, 3–8 August 2008, AIP publishers, Melville NY, USA, 31–34, 2009. 9649, 9651

Chevalier, F.: Sampled database of 60 levels atmospheric profiles from the ECMWF analysis, Tech. Rep., ECMWF EUMETSAT SAF programme Research Report 4, 2001. 9656

Clough, S. A., Kneizys, F. X., and Davies, R. W.: Line shape and the water vapor continuum, Atmos. Res., 23, 229–241, 1989. 9651

Clough, S. A., Shephard, M. W., Mlawer, E. J, Delamere, J. S., Iacono, M. J., Cady-Pereira, K., Boukabara, S., and Brown, P. D.: Atmospheric radiative transfer modeling: a summary of the AER codes, J. Quant. Spectrosc. Ra., 91, 233–244, doi:10.1016/j.jqsrt.2004.05.058, 2005. 9651

Cousins, D. and Gazarick, M. J.: NAST Interferometer Design and Characterization, Final Report, MIT Lincoln Laboratory Project Report NOAA-26, 13 July 1999. 9650

Eremenko, M., Dufour, G., Foret, G., Keim, C., Orphal, J., Beekmann, M., Bergametti, G., and Flaud, J.-M.: Tropospheric ozone distributions over Europe during the heat wave in July 2007 observed from infrared nadir spectra recorded by IASI, Geophys. Res. Lett., 35, L18805, doi:10.1029/2008GL034803, 2008. 9659

EUMETSAT: IASI science plan, EUMETSAT, Darmstadt, 1998.

Gordon, I. E., Rothman, L. S., Gamache, R. R., Jacquemart, D., Boone, C., Bernath, P. F., Shephard, M. W., Delamere, J. S., and Clough, S. A.: Current updates of the water-vapor line list in HITRAN: A new diet for air-broadened half-widths, J. Quant. Spectrosc. Ra., 108, 389–402, doi:10.1016/j.jqsrt.2007.06.009, 2007. 9649, 9652

Grieco, G., Luchetta, A., Masiello, G., Serio, C., and Viggiano, M.: IMG O_3 retrieval and comparison with TOMS/ADEOS columnar ozone: an analysis based on tropical soundings, J. Quant. Spectrosc. Ra., 95, 331–348, 2005. 9651, 9654

Grieco, G., Masiello, G., Matricardi, M., Serio, C., Summa, D., and Cuomo, V.: Demonstration and validation of the φ-IASI inversion scheme with NAST-I data, Q. J. Roy. Meteor. Soc., 133(S3), 217–232, 2007. 9648, 9650, 9651, 9653, 9654, 9658, 9660

Hansen, C.: Analysis of discrete ill-posed problems by means of the L-curve, SIAM Rev., 34(4), 561–580, doi:10.1137/1034115, 1992. 9654

Masiello, G., Serio, C., and Shimoda, H.: Qualifying IMG Tropical Spectra for Clear Sky, J. Quant. Spectrosc. Ra., 77(2), 131–148, 2003. 9650, 9660

Masiello, G. and Serio, C.: An effective water vapour self-broadening scheme for look-up-table based radiative transfer, in: Remote Sensing of Clouds and the Atmosphere VII Proceedings of SPIE, Agia Pelagia, Crete, Greece, 24–28 September 2002, Bellingham, Washington, USA, 4882, 52–61, doi:10.1117/12.462580, 2003. 9651

Masuda, K., Takashima, T., and Takayama, Y.: Emissivity of pure and sea waters for the model sea surface in the infrared window regions, Remote Sens. Environ., 24, 313–329, 1988. 9657

Niro, F., Jucks, K., and Hartmann, J.-M.: Spectra calculations in central and wing regions of CO_2 IR bands, IV : Software and database for the computation of atmospheric spectra, J. Quant. Spectrosc. Ra., 95, 469–481, doi:10.1016/j.jqsrt.2004.11.011, 2005. 9652, 9663

Rodgers, C. D.: Retrieval of atmospheric temperature and composition from remote measurements of thermal radiation, Rev. Geophys. Space Ge., 14, 609–624, 1976. 9654

Rothman, L. S., Barbe, A., Benner, D. C., Brown, L. R., Camy-Peyret, C., Carleer, M. R., Chance, K., Clerbaux, C., Dana, V., Devi, V. M., Fayt, A., Flaud, J.-M., Gamache, R. R., Goldman, A., Jacquemart, D., Jucks, K. W., Lafferty, W. J., Mandin, J.-Y., Massie, S. T., Nemtchinov, V., Newnham, D. A., Perrin, A., Rinsland, C. P., Schroeder, J., Smith, K. M., Smith, M. A. H., Tang, K., Toth, R. A., Vander Auwera, J., Varanasi, P., and Yoshino, K.: The HITRAN molecular spectroscopic database: edition of 2000 including updates through 2001, J. Quant. Spectrosc. Ra., 82, 5–44, doi:10.1016/S0022-4073(03)00146-8, 2003. 9649, 9652

Rothman, L. S., Jacquemart, D., Barbe, A., Benner, D. C., Birk, M., Brown, L. R., Carleer, M. R., Chackerian, C., Chance, K., Coudert, L. H., Dana, V., Devi, V. M., Flaud, J. M., Gamache, R. R., Goldman, A., Hartmann, J. M., Jucks, K. W., Maki, A. G., Mandin, J. Y., Massie, S. T., Orphal, J., Perrin, A., Rinsland, C. P., Smith, M. A. H., Tennyson, J., Tolchenov, R. N., Toth, R. A., Vander Auwera, J., Varanasi, P., and Wagner, G.: The HITRAN 2004 molecular spectroscopic database, J. Quant. Spectrosc. Ra., 96, 139–204, doi:10.1016/j.jqsrt.2004.10.008, 2005. 9649, 9652

Saunders, R., Rayer, P., Brunel, P., von Engeln, A., Bormann, N., Strow, L., Hannon, S., Heilliette, S., Liu, X., Miskolczi, F., Han, Y., Masiello, G., Moncet, J. L., Uymin, G., Sherlock, V., and Turner, S. D.: A comparison of radiative transfer models for simulating Atmospheric Infrared

Sounder (AIRS) radiances, J. Geophys. Res., 112, D01S90, doi:10.1029/2006JD007088, 2007. 9650

Serio, C., Masiello, G., and Grieco, C.: EOF regression analytical model with applications to the retrieval of atmospheric temperature and gas constituents concentration from high spectral resolution infrared observations, in: Environmental Modelling: New Research, edited by: Findley, P. N., Nova Science Publishers, Inc., Hauppagauge, NY, USA, 51–88, ISBN: 978-1-60692-034-3, 2009. 9651, 9654, 9659

Serio, C., Esposito, F., Masiello, G., Pavese, G., Calvello, M. R., Grieco, G., Cuomo, V., Buijs, H. L., and Roy, C. B.: Interferometer for ground-based observations of emitted spectral radiance from the troposphere: evaluation and retrieval performance, Appl. Optics, 47(21), 3909–3919, 2008. 9659

Shephard, M. W., Clough, S. A., Payne, V. H., Smith, W. L., Kireev, S., and Cady-Pereira, K. E.: Performance of the line-by-line radiative transfer model (LBLRTM) for temperature and species retrievals: IASI case studies from JAIVEx, Atmos. Chem. Phys. Discuss., 9, 9313–9366, 2009, http://www.atmos-chem-phys-discuss.net/9/9313/2009/. 9665, 9668

Taylor, J. P.: Principal Investigator, Joint Airborne IASI Validation Experiment, available at: http://badc.nerc.ac.uk/data/jaivex/. 9648, 9660

Taylor, J. P., Smith, W. L., Cuomo, V., Larar, A. M., Zhou, D. K., Serio, C., Maestri, T., Rizzi, R., Newman, S., Antonelli, P., Mango, S., Di Girolamo, P., Esposito, F., Grieco, G., Summa, D., Restieri, R., Masiello, G., Romano, F., Pappalardo, G., Pavese, G., Mona, L., Amodeo, A., and Pisani, G.: EAQUATE An International Experiment For Hyper-spectral Atmospheric Sounding Validation, B. Am. Meteorol. Soc., 89(2), 203–218, doi:10.1175/BAMS-89-2-203, 2008. 9650

Tobin, D. C., Best, F. A., Brown, P. D., Clough, S. A., Dedecker, R. G., Ellingson, R. G., Garcia, R. K., Howell, H. B., Knuteson, R. O., Mlawer, E. J., Revercomb, H. E., Short, J. F., van Delst, P. F. W., and Walden, V. P.: Downwelling spectral radiance observations at the SHEBA ice station: Water vapor continuum measurements from 17 to 26 μm, J. Geophys. Res., 04(D2), 2081–2092, 1999. 9652

Zhou, D. K., Smith, W. L., Larar, A. M., Liu, X., Taylor, J. P., Schlüssel, P., Strow, L. L., and Mango, S. A.: All weather IASI single field-of-view retrievals: case study – validation with JAIVEx data, Atmos. Chem. Phys., 9, 2241–2255, 2009, http://www.atmos-chem-phys.net/9/2241/2009/. 9669

Table 1. Definition of σ-IASI pressure levels.

Layer	Pressure [hPa]	Layer	Pressure [hPa]	Layer	Pressure [hPa]
1	1013–1005	21	550–500	41	55.3–53.2
2	1005–1000	22	500–466	42	53.2–51.1
3	1000–986	23	466–432	43	51.1–50.0
4	986–973	24	432–400	44	50.0–48.8
5	973–960	25	400–350	45	48.8–47.3
6	960–946	26	350–300	46	47.3–45.8
7	946–933	27	300–275	47	45.8–40.0
8	933–925	28	275–250	48	40.0–30.0
9	925–913	29	250–225	49	30.0–25.0
10	913–900	30	225–200	50	25.0–20.0
11	900–875	31	200–175	51	20.0–15.0
12	875–850	32	175–150	52	15.0–10.0
13	850–833	33	150–122	53	10.0–7.0
14	833–814	34	122–100	54	7.0–5.0
15	814–795	35	100–85	55	5.0–3.0
16	795–748	36	85–70	56	3.0–2.0
17	748–700	37	70–65	57	2.0–1.0
18	700–650	38	65–60	58	1.0–0.5
19	650–600	39	60–57.5	59	0.5–0.1
20	600–550	40	57.5–55.3	60	0.1–0.005

ACPD
9, 9647–9691, 2009

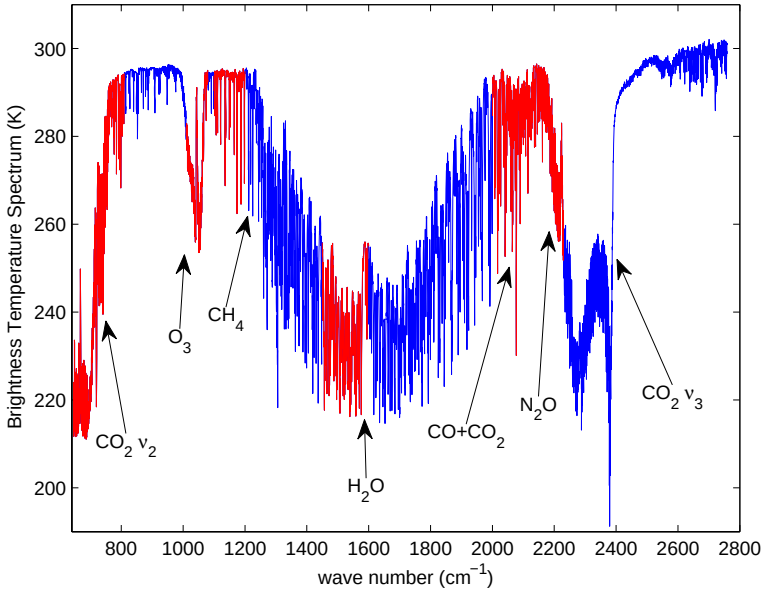

Fig. 1. Example of IASI spectrum (in units of brightness temperature) showing (in red) the spectral ranges or channels used for inversion of temperature, water vapour and ozone profiles. The spectrum has been recorded on 29 April 2009 in the Gulf of Mexico during the JAIVEx campaign.

ACPD
9, 9647–9691, 2009

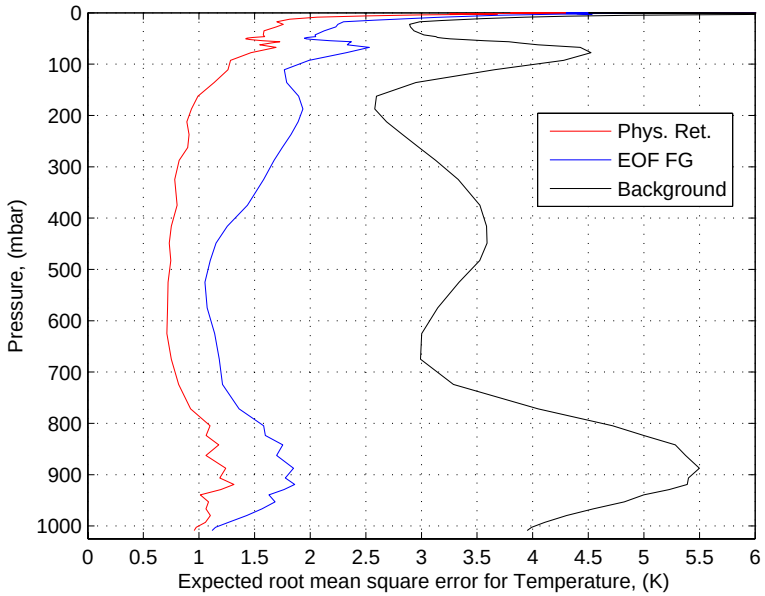

Fig. 2. Expected IASI temperature retrieval accuracy for tropical soundings. The figure compares the accuracy provided by the mean value of the training data set (computed as standard deviation of the ensemble of test profiles, this is referred to as background in figure) to the two ones obtained with the EOF regression scheme, and finally the physical inversion, respectively.

ACPD
9, 9647–9691, 2009

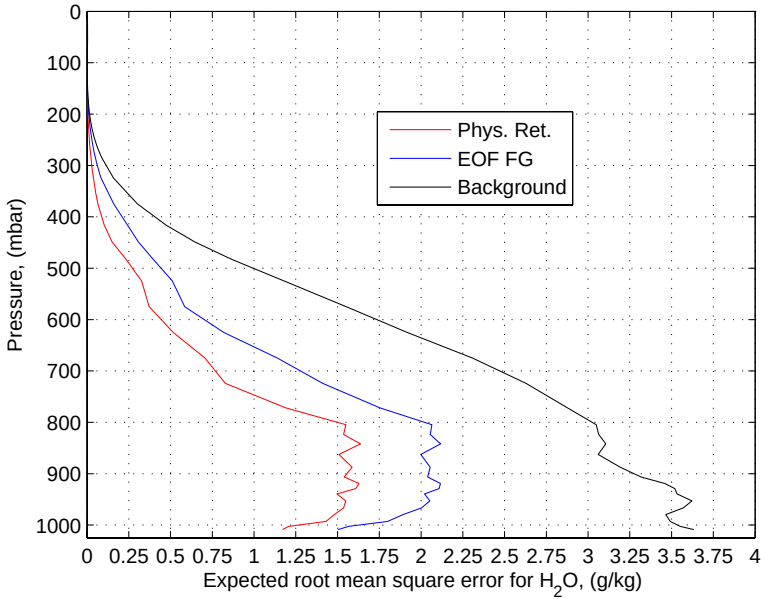

Fig. 3. As Fig. 2, but for water vapour.

ACPD
9, 9647–9691, 2009

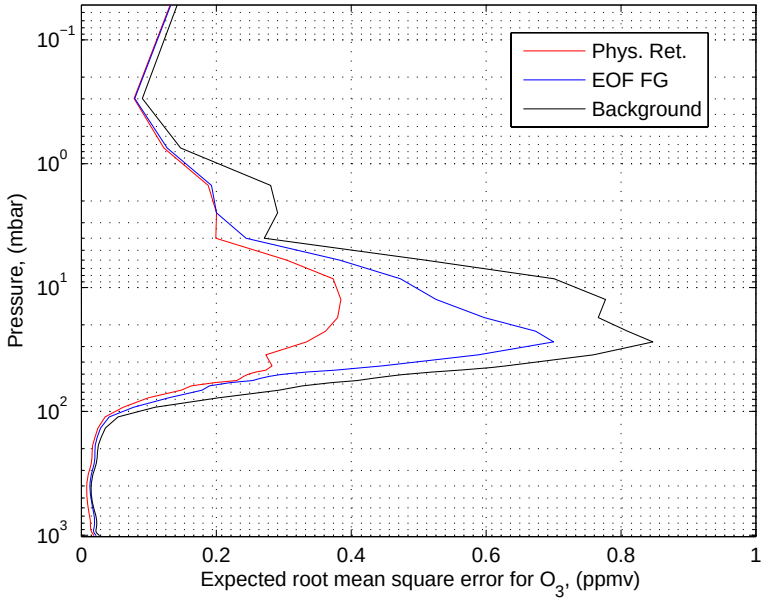

Fig. 4. As Fig. 2, but for ozone.

ACPD
9, 9647–9691, 2009

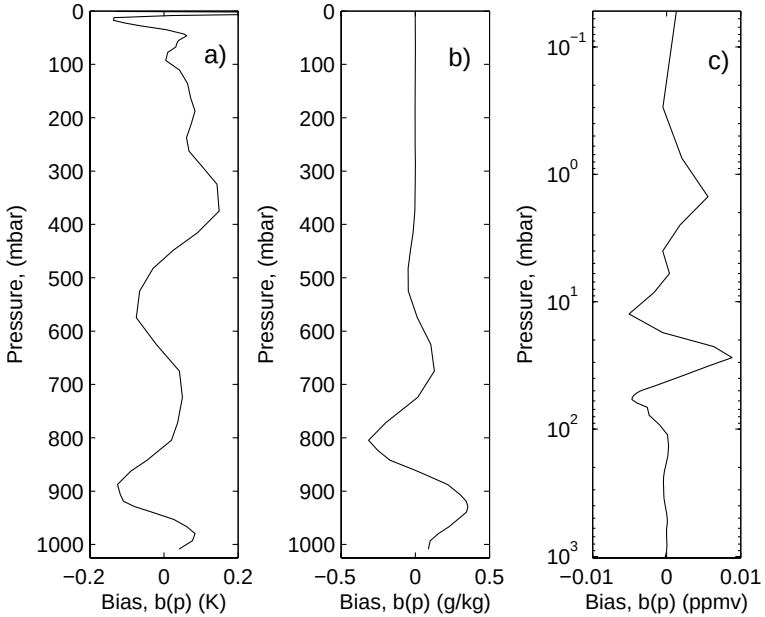

Fig. 5. Bias, indicated as $b(p)$ in figure, for the physical retrieval for **(a)** temperature, **(b)** water vapour, **(c)** ozone. Note the logarithmic scale for the pressure axis in the case of ozone.

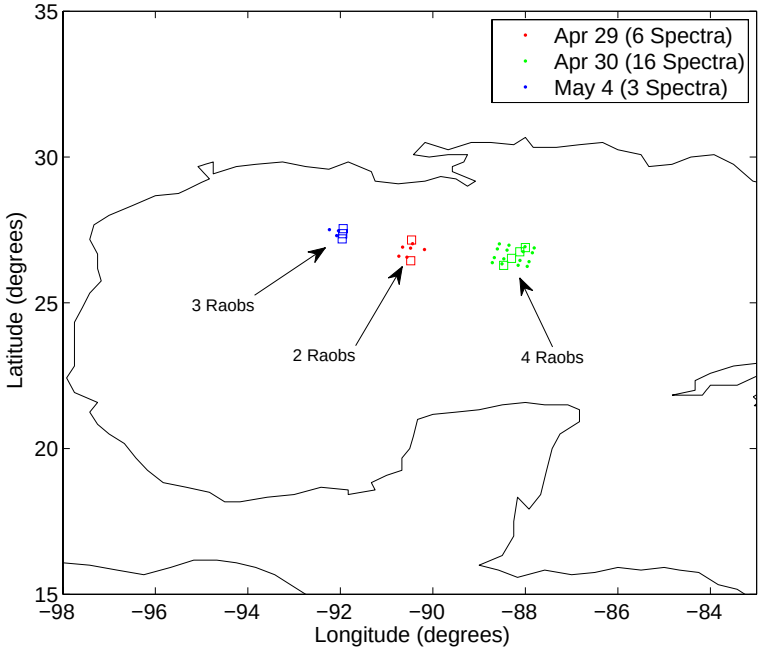

Fig. 6. IASI footprints and radiosonde observations for the JAIVEx data used in this paper.

ACPD
9, 9647–9691, 2009

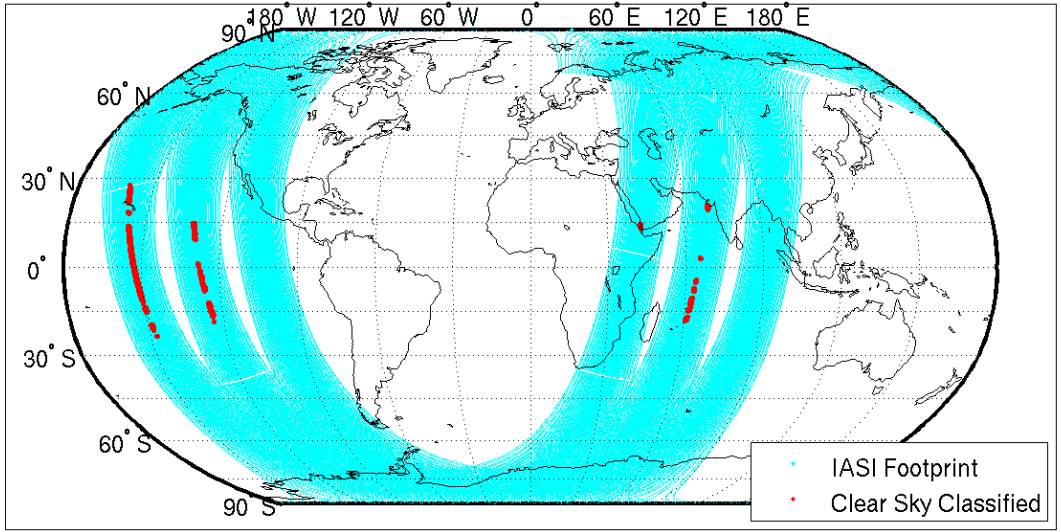

Fig. 7. IASI orbits for the day 22 July 2007 and clear sky footprints (in red) considered in this analysis.

ACPD
9, 9647–9691, 2009

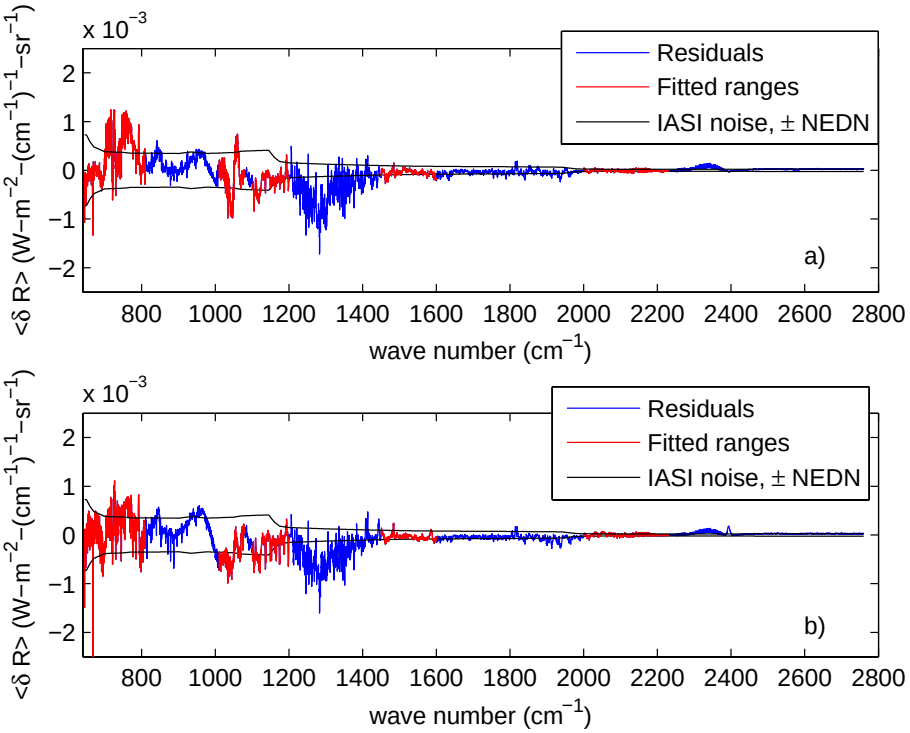

Fig. 8. Spectral residual, δ**R** averaged over the 25 JAIVEx IASI soundings analyzed in this paper. **(a)** spectral residual for the case L8.1, **(b)** spectral residual for the case L11.3. The residuals in red corresponds to the spectral ranges, which have been used in the inversion process.

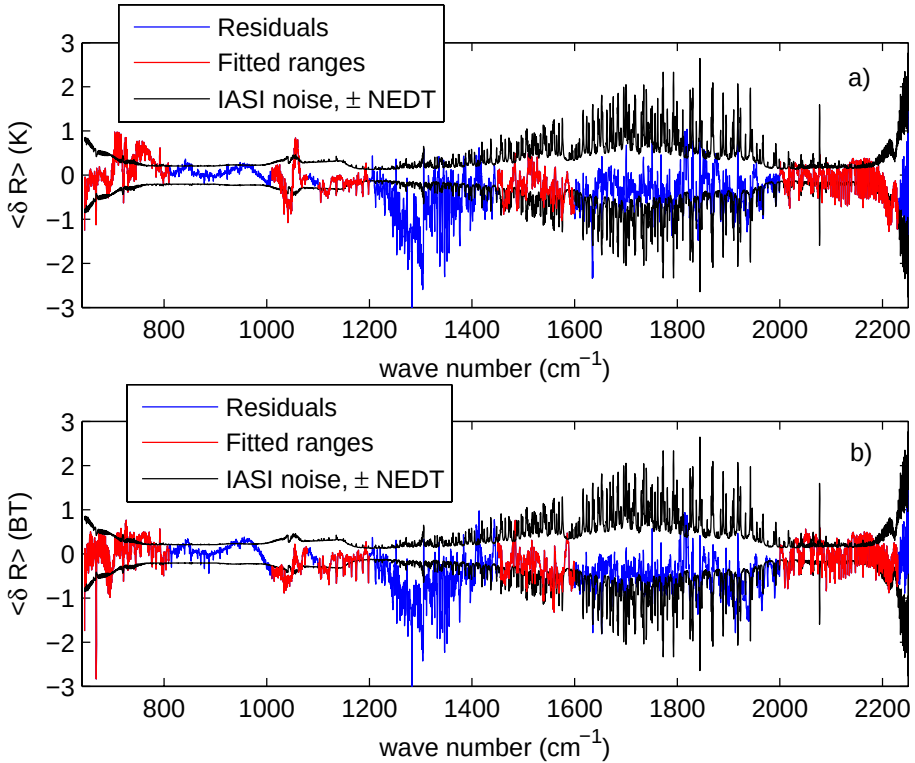

Fig. 9. As Fig. 8, but in units of brightness temperature (K). To improve reading, only the spectral coverage of interest to inversions for geophysical parameters is shown.

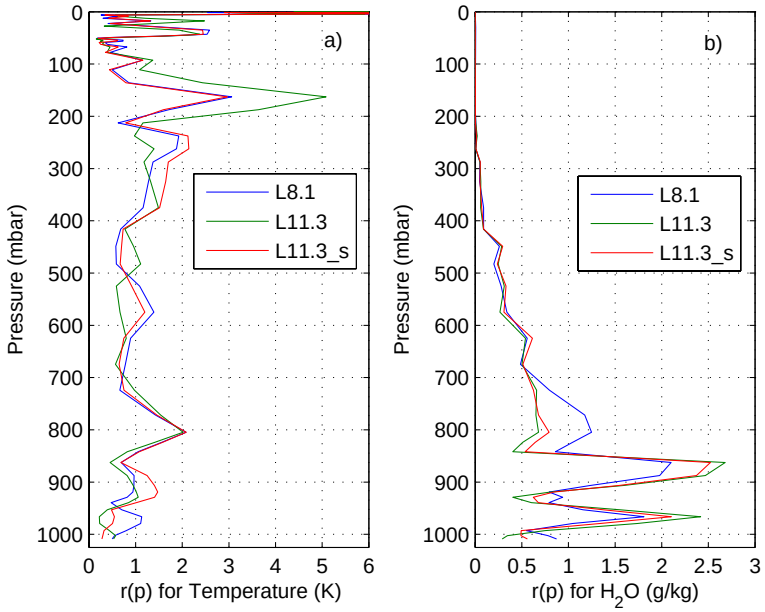

Fig. 10. JAIVEx experiment. Root mean square difference (r in figure) computed by contrasting IASI retrievals against radiosonde observations for the day 30 April 2007. Values have been averaged over the data set of 16 IASI soundings. **(a)** temperature; **(b)** water vapour. The three r-curves shown in figure correspond to the three versions of σ-IASI used in the analysis (see text for discussion).

ACPD
9, 9647–9691, 2009

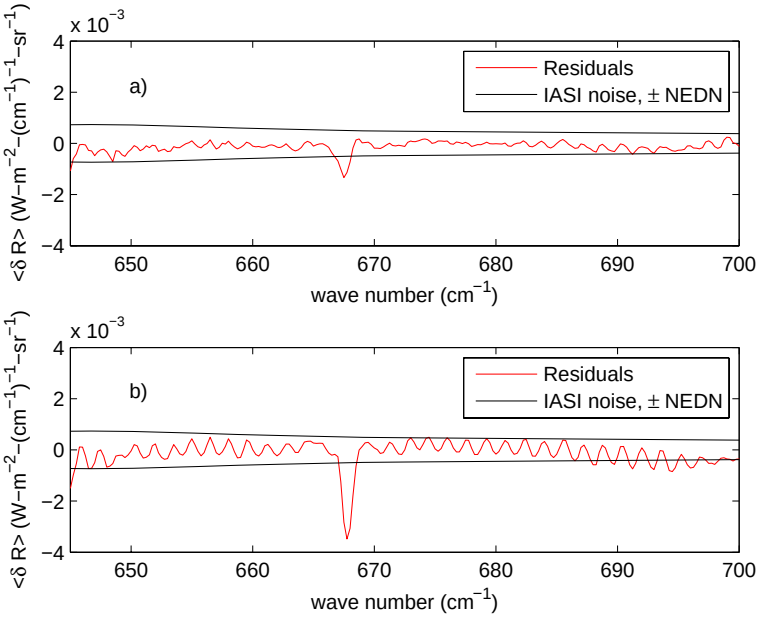

Fig. 11. As Fig. 8, but now only the spectral range 645 to 700 cm^{-1} is shown. **(a)** spectral residual for the case L8.1, **(b)** spectral residual for the case L11.3.

ACPD
9, 9647–9691, 2009

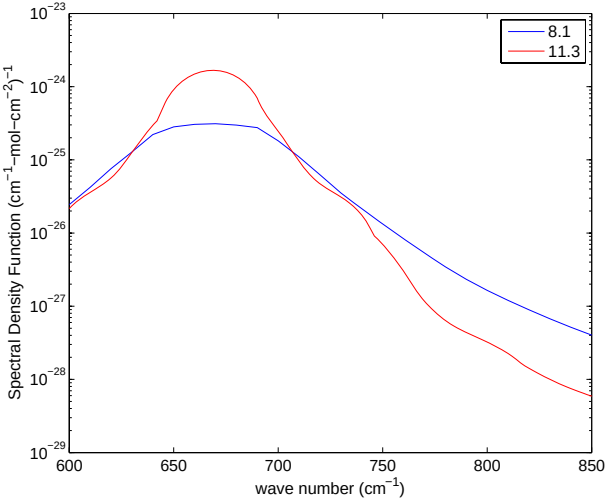

Fig. 12. Exemplifying the CO_2 continuum absorption coefficient behaviour as modelled by LBLRTM version 8.1 and 11.3. The spectral density function is plotted in figure for the CO_2 ν_2 band.

ACPD
9, 9647–9691, 2009

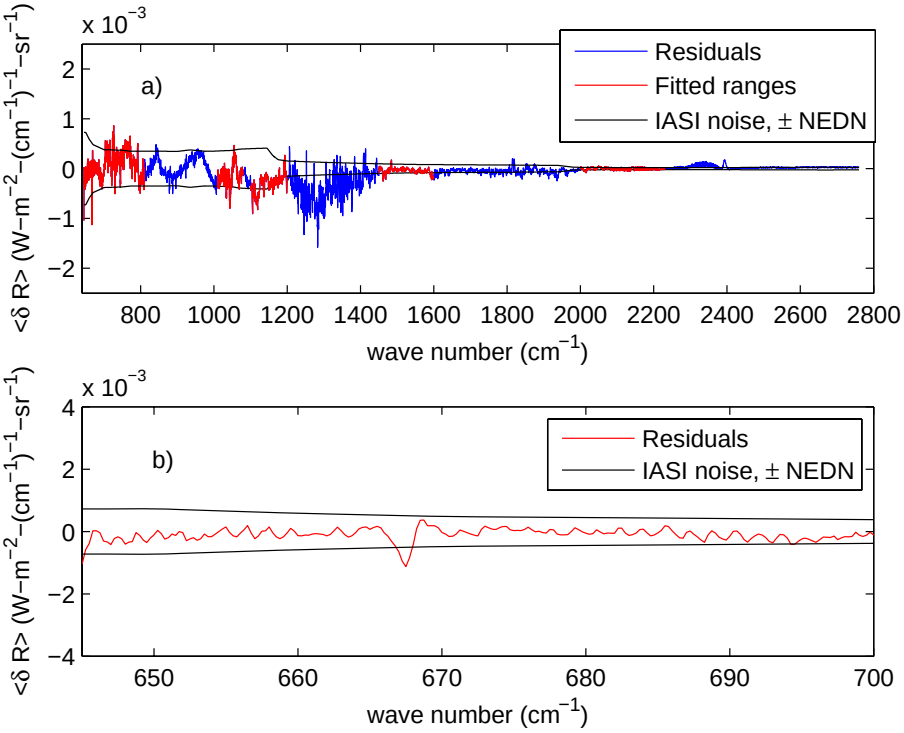

Fig. 13. Spectral residual, $\delta\mathbf{R}$ averaged over the 25 JAIVEx IASI soundings analyzed in this paper for the case L11.3_s. **(a)** spectral residual over the full IASI spectral coverage; **(b)** spectral residual for the range 645 to 700 cm^{-1}.

ACPD
9, 9647–9691, 2009

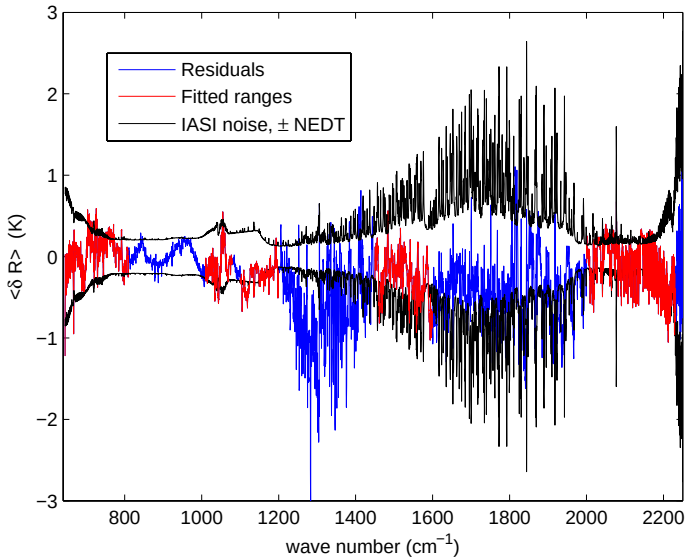

Fig. 14. As Fig. 13a, but in units of brightness temperature. To improve reading, only the spectral coverage of interest to inversions for geophysical parameters is shown.

ACPD
9, 9647–9691, 2009

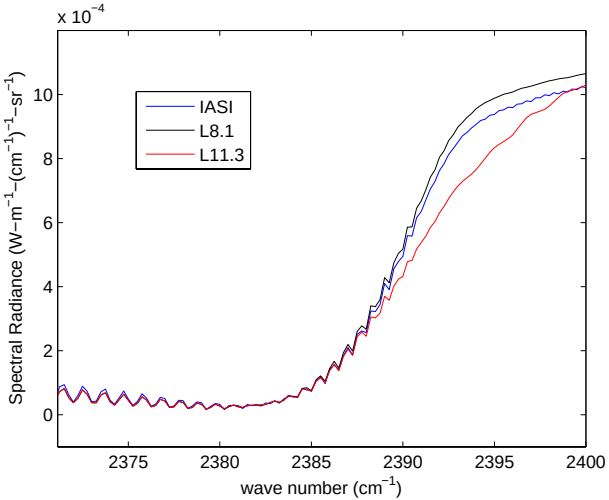

Fig. 15. IASI and fitted spectra (averaged over the 25 JAIVEx IASI soundings) for the two cases L8.1 and L11.3 at the CO_2 ν_3 band head, showing the relevant inconsistency of L11.3 when compared to the IASI observations.

ACPD
9, 9647–9691, 2009

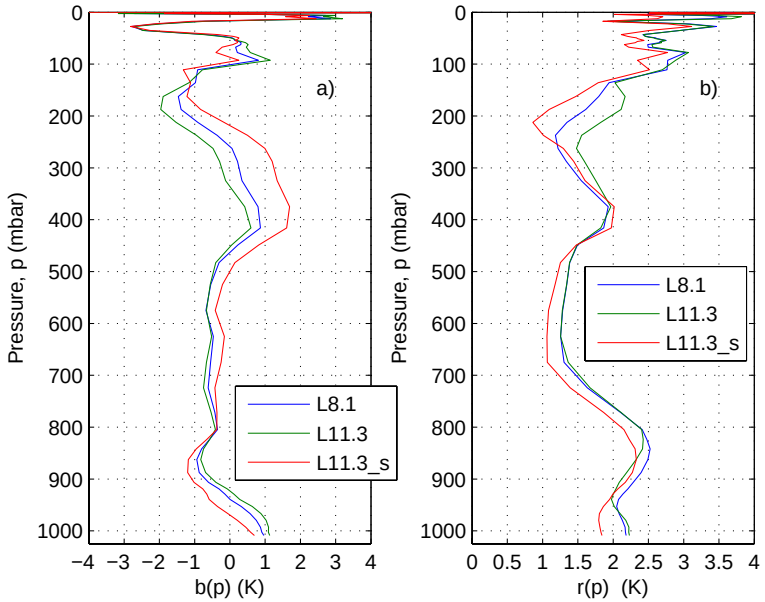

Fig. 16. Averaged linear difference (*b* in figure) and root mean square difference (*r* in figure) between IASI temperature retrieval and ECMWF. Values have been averaged over the full tropical data set of 647 IASI soundings. All the three results obtained with the three versions L8.1, L11.3 and L11.3_s are shown.

ACPD
9, 9647–9691, 2009

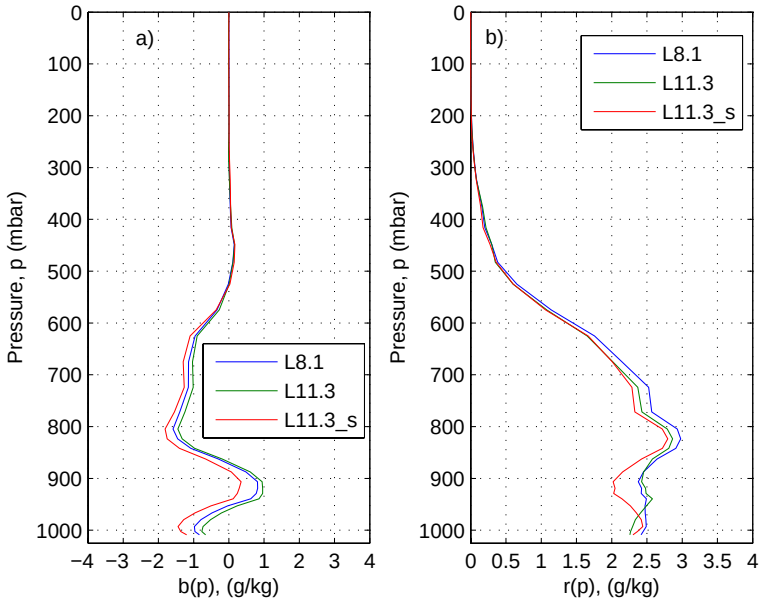

Fig. 17. As Fig. 16, but for water vapour.

ACPD
9, 9647–9691, 2009

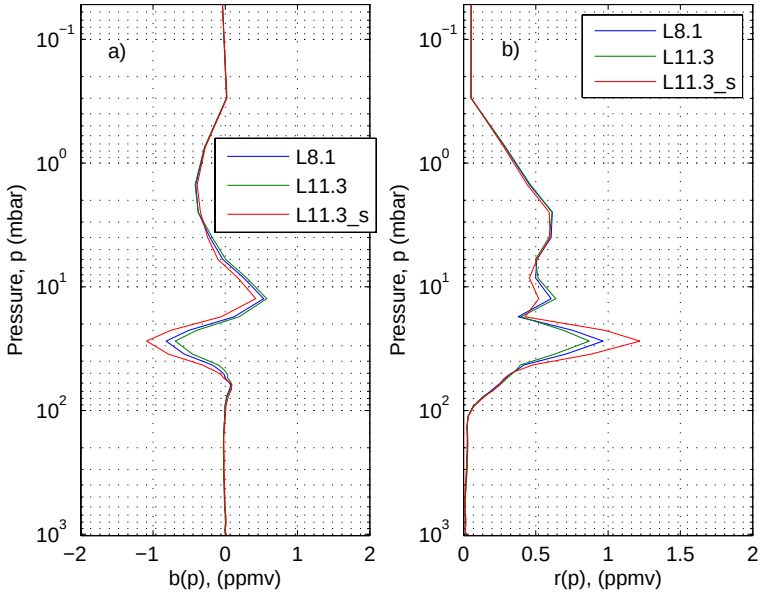

Fig. 18. As Fig. 16, but for ozone.

ACPD
9, 9647–9691, 2009